

Natural frequencies and response amplitude operators of scale model of spar-type floating offshore wind turbine

Sin-Pyo Hong^{1a} and Jin-Rae Cho^{*2}

¹Global Core Research Center for Ships and Offshore Plants, Pusan National University, Busan 609-735, Republic of Korea

²Department of Naval Architecture and Ocean Engineering, Hongik University, Sejong 339-701, Republic of Korea

(Received March 26, 2016, Revised October 27, 2016, Accepted December 7, 2016)

Abstract. This paper is concerned with the comparative numerical and experimental study on the natural behavior and the motion responses of a 1/75 moored scale model of a 2.5 MW spar-type floating offshore wind turbine subject to 1-D regular wave. Heave, pitch and surge motions and the mooring tensions are investigated and compared by numerical and experimental methods. The upper part of wind turbine which is composed of three rotor blades, hub and nacelle is modeled as a lumped mass and three mooring lines are pre-tensioned by means of linear springs. The numerical simulations are carried out by a coupled FEM-cable dynamics code, while the experiments are performed in a wave tank equipped with the specially-designed vision and data acquisition system. Using the both methods, the natural behavior and the motion responses in RAOs are compared and parametrically investigated to the fairlead position, the spring constant and the location of mass center of platform. It is confirmed, from the comparison, that both methods show a good agreement for all the test cases. And, it is observed that the mooring tension is influenced by all three parameters but the platform motion is dominated by the location of mass center. In addition, from the sensitivity analysis of RAOs, the coupling characteristic of platform motions and the sensitivities to the mooring parameters are investigated.

Keywords: spar-type floating platform; scale model; natural frequencies; response amplitude operator (RAO); mooring tension; center of mass; fairlead position; spring constant

1. Introduction

Above-ground wind turbines showed the rapid advance in both the total installation number and the maximum power capacity to some extent. But, such a continuous increase has been slowed down owing to the several critical obstacles, such as the substantial environmental impact on people living in the vicinity of wind turbines and the limitation in making a wind farm. For this reason, offshore wind turbines that could be installed at the offshore sites, a less restrictive installation place, are intensively and globally receiving attention. Offshore wind turbines are basically classified into fixed- and floating-type depending on the supporting methodology of the wind turbine tower. Differing from the fixed-type, the floating-type has not been really commercialized because several core technologies are not fully settled down (Karimirad *et al.* 2011), particularly the securing of the dynamic performance to the wind, wave and current loads (Faltinsen 1990). Here, the dynamic performance is mostly meant by the station keeping at sea and the suppression of rotational oscillation (Tong 1998).

Floating offshore wind turbines are in turn classified into, according to how is generated the righting moment or draft control, semi-submersible, TLP (tension-leg platform)-

type, spar-types (Lee 2008, Jonkman 2009, Sultania and Mauel 2016), and barge-type. However, all the types have some things in common from the fact that the dynamic performance to wind and wave excitations is evaluated in terms of the rigid body motions of floating substructure. The station keeping at sea is evaluated mostly by two translation motions; surge and sway, while the vertical and rotational oscillation are mostly by heave, pitch and roll motions. In case of spar-type floating wind turbine, the buoyancy produced by a long hollow cylindrical platform supports the whole offshore wind turbine and the mooring lines keep the station position. The dynamic response and station keeping are influenced by the fairlead position and the cable length and tension (Jeon *et al.* 2013) as well as the type and configuration of mooring lines (Sannasiraj *et al.* 1998).

On the other hand, it has been reported that the rotational oscillation tends to become larger in proportional to the metacentric height (i.e., the relative vertical distance between the metacenter and the center of mass) and the relative distance between the center of gravity and the center of buoyancy (Koo *et al.* 2004). Karimirad *et al.* (2011) considered a single tendon mooring system and noticed that the restoring force from the tendon should be included in the restoring stiffness of the floating platform in pitch, roll and heave. But, if a catenary mooring system is used, its contribution to the restoring stiffness in these three motion modes is small enough to neglect. Meanwhile, the rotational oscillation is also influenced by both the fairlead position of mooring lines and the mooring tension, and it

*Corresponding author, Professor

E-mail: jrcho@hongik.ac.kr

^aResearch Professor

could be improved further when passive tuned liquid damper (TLD) or/and active posture control devices employed (Lee 2005, Lee *et al.* 2006, Colwell *et al.* 2009, Dinh *et al.* 2016). Here, the pitch and roll stiffness is meant by the pitching and rolling moments required to pitch and roll the substructure by unit angle.

Regarding the floating-type offshore wind turbines, there have been many research works on the motion responses to the above-mentioned parameters. According to our literature survey, Utsunomiya (2010), Goopee *et al.* (2012), Mostafa *et al.* (2012) performed the experimental studies using scale models. And, Shin and Dam (2012) presented the experimental results for a floating offshore wind turbine moored by a spring-tensioned leg. Martin *et al.* (2012), Fowler *et al.* (2013) developed the state-of-the-art model test technique to physically represent a wind turbine in the model test environment. Meanwhile, Karimirad (2010), Jensen *et al.* (2011), Dodaran and Park (2012) presented the theoretical studies by simplifying the wind turbine geometry, by deriving wind and wave loads and by developing the design analysis of mooring system. The studies were also made by the combined use of CFD, hydro, FSI (fluid-structure interaction) or/and MBD (multibody dynamics) codes (Zambrano *et al.* 2006, Jonkman 2009, Jonkman and Musial 2010, Wang and Sweetman 2012, Choi *et al.* 2015).

Even though the researches on floating offshore wind turbine have been actively conducted, the detailed useful results for the design of spar-type floating platform to the key design parameters are still in need of further investigation. Furthermore, the reliability of numerical and experimental results is also in doubt, in particular when the results are not validated through the comparison between the numerical simulation and the experiment. In this context, the ultimate goal of our study is to establish a comparative numerical-experimental method for securing the reliability of useful simulation and test data to the key design parameters. As a preliminary step for our goal, we in this study consider the natural and dynamic behaviors, such as surge, pitch and heave motions, of 2.5MW spar-type floating offshore wind turbine that is subject to 1-D regular wave load. By restricting to the wave load, the upper part including rotor blades, hub and nacelle is simplified as a lumped mass.

For the comparative numerical and experimental study, a 1/75 scale model is used, and the location of mass center of platform, the fairlead position and the spring constant of mooring cables are chosen as three key parameters. A vision and data acquisition system is specially designed to accurately measure the natural and dynamic motions of scale model in a wave tank. Meanwhile, the numerical simulation is performed by the fluid-cable dynamics interaction method. Four test cases are designed by appropriately combining three design parameters, and then the natural frequencies and RAOs of the spar floating platform and the mooring tension are compared and investigated. As well, the sensitivity of RAOs to the mooring system is evaluated. Through the comparative and parametric studies, the matching between the numerical and experimental methods is examined and the effects of three

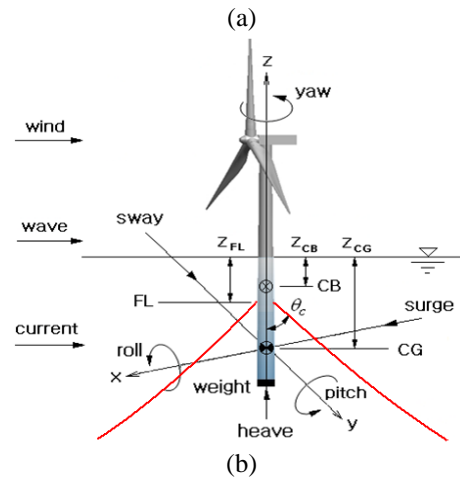


Fig. 1 (a) Spar-type floating offshore wind turbine (b) 6-DOF rigid body motions (CB: center of buoyancy, CG: center of gravity, FL: fairlead)

key design parameters on RAOs and their sensitivities are profoundly investigated.

2. Dynamic response of spar-type floating offshore wind turbine

Fig. 1(a) shows a typical spar-type floating offshore wind turbine stationed by a bottom weight and three mooring cables which are anchored at seabed and connected to the fairlead of floating platform. The mooring system is usually composed of fabric ropes and steel chains for the sake of the topological simplicity and cost effectiveness (Wu 1995). The mooring cables are subject to the self-weight, the hydrodynamic drag forces and the added inertia force (Vaz and Patel 2000), but they resist to only the in-line tension because of its small flexural rigidity. Fig. 1(b) represents the key parameters associated with the dynamic performance, as well as six rigid body motions of the floating platform. The dynamic performance of floating platform may not only influence the structural safety of whole wind turbine, but it may also degrade the wind power efficiency because of the misalignment of rotor blades to the wind direction. Hence, it becomes the most important subject at the design stage and in the maintenance of floating offshore wind turbine.

The mooring system, which plays an important role in both the station keeping and the suppression of rotational

oscillation, is characterized by its tension and fairlead location. The mooring tension is influenced by the total cable length and the installation angle θ_c as well as the specific weight and the cable stiffness. Here, it has been reported that the mooring line tension decreases in proportional to the total suspended cable length, and it becomes almost insensitive to the total cable length once the total suspended length reaches a critical portion (Jeon *et al.* 2013). Meanwhile, the rotational stability of wind turbine, which is mostly related to roll and pitch motions, is greatly influenced by the fairlead position Z_{FL} and the pitch and roll stiffness of floating platform. In general, the pitch and roll stiffness of floating platform is determined by the center of buoyancy (CB) and the center of gravity (CG), and it is proportional to the metacentric height (Karimirad *et al.* 2011). Thus, these key parameters should be appropriately chosen to maximize the dynamic performance of spar-type floating offshore wind turbine, which could be made based on its dynamic response analyses.

Referring to Fig. 2(a), let us $\Omega_F \in \mathcal{R}^3$ be a semi-infinite unbounded flow domain with the boundary $\partial\Omega_F = \overline{S_F \cup S_B \cup \Gamma_I}$ and denote \mathbf{V} be a continuous triple-vector water velocity field, where S_F , S_B and Γ_I indicate the free surface, seabed and flow-structure interface respectively. Water is assumed to be inviscid and incompressible and water flow is irrotational so that there exists a velocity potential function $\phi(\mathbf{x};t)$ satisfying $\phi(\mathbf{x};t) \cdot \mathbf{V} = \nabla\phi$. Here, the velocity potential function $\phi(\mathbf{x};t)$ is defined by

$$\phi(\mathbf{x};t) = \sum_{j=1}^6 \phi_j + \phi_w + \phi_d \quad (1)$$

with ϕ_j due to the rigid body motion of structure, ϕ_w due to undisturbed incoming wave and ϕ_d due to diffraction of the undisturbed incoming wave, respectively. Then, the flow field is governed by the continuity equation

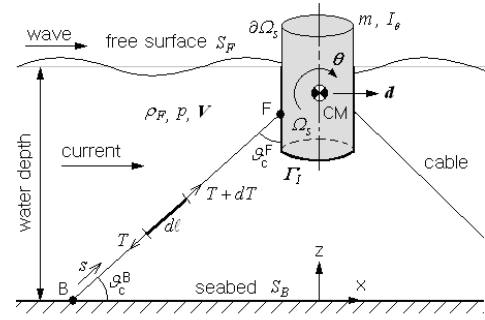
$$\nabla^2\phi = 0, \quad \text{in } \Omega_F \times (0, \hat{t}] \quad (2)$$

and the fluid-structure interaction condition given by

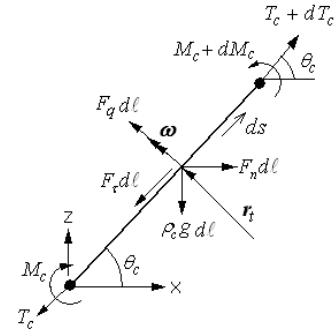
$$\frac{\partial\phi}{\partial n} = \dot{\mathbf{u}} \cdot \mathbf{n}, \quad \text{on } \Gamma_I \quad (3)$$

together with the unified free surface condition on S_F (Cho *et al.* 2005) and the zero normal velocity on the seabed S_B . Here, \hat{t} is the time period of observation, \mathbf{u} the rigid body displacement of platform, g the gravity acceleration, and \mathbf{n} the outward unit vector normal to the platform boundary. In addition, the potential function satisfies the radiation condition: $\phi \rightarrow 0$ as $r \rightarrow \infty$ at the far field.

Meanwhile, the floating platform occupying the material domain $\Omega_S \in \mathcal{R}^3$ with the boundary $\partial\Omega_S$ is assumed to be a rigid body. By denoting $\{\mathbf{d}(\mathbf{x};t), \boldsymbol{\theta}(\mathbf{x};t)\} = \{\bar{\mathbf{d}}(\mathbf{x}), \bar{\boldsymbol{\theta}}(\mathbf{x})\} e^{j\omega t}$ be its rigid body translation and rotation at the center of mass, the dynamic motion of the platform is governed by the conservation of linear and angular momentums in the frequency domain, respectively



(a)



(b)

Fig. 2 (a) A moored rigid spar floating platform in regular wave (b) forces acting on the cable element

$$(-\omega^2 m[\mathbf{I}] + j\omega[\mathbf{c}] + [\mathbf{k}])\{\bar{\mathbf{d}}\} = \{\bar{\mathbf{F}}\}, \quad \text{in } \Omega_S \quad (4)$$

$$(-\omega^2 [\mathbf{I}^\theta] + j\omega[\mathbf{c}^\theta] + [\mathbf{k}^\theta])\{\bar{\boldsymbol{\theta}}\} = \{\bar{\mathbf{M}}\}, \quad \text{in } \Omega_S \quad (5)$$

and the initial conditions given by

$$\{\dot{\mathbf{d}}, \dot{\boldsymbol{\theta}}\}_{t=0} = \{\dot{\mathbf{d}}_0, \dot{\boldsymbol{\theta}}_0\}, \quad \{\mathbf{d}, \boldsymbol{\theta}\}_{t=0} = \{\mathbf{d}_0, \boldsymbol{\theta}_0\} \quad (6)$$

with the imaginary unit j and the notation convention $[\mathbf{A}] = \text{diag}(A_x, A_y, A_z)$ for four matrices $[\mathbf{c}]$, $[\mathbf{k}]$, $[\mathbf{c}^\theta]$ and $[\mathbf{k}^\theta]$. Here, m, c_i, k_i, c_i^θ and k_i^θ denote the total mass and the damping and stiffness coefficients for the translational and rotational degrees of freedom, respectively. Meanwhile, $[\mathbf{I}^\theta]$ indicates the matrix of mass moments of inertia with respect to the center of mass, and $\bar{\mathbf{F}}$ and $\bar{\mathbf{M}}$ are the pressure-induced external force and moment which are calculated in terms of the hydrodynamic pressure p and the position vector r from the center of mass.

Meanwhile, mooring cables of length L are a slender flexible structure subject to hydrodynamic pressure, self-weight, inertia and drag forces. Referring to Fig. 2(b), the nonlinear differential equations of motion (Goodman and Breslin 1976, Aamo and Fossen 2000) for the differential cable element with the length dl are governed by the equilibrium equations in translation and rotation

$$(m_c + m_a) \frac{\partial \dot{\mathbf{u}}_c}{\partial t} = \frac{\partial \mathbf{T}_c}{\partial s} + (1 + \gamma) \mathbf{F}_c \quad (7)$$

$$\frac{\partial \mathbf{M}_c}{\partial s} = -\mathbf{r}_t \times (1 + \gamma) \mathbf{T}_c \quad (8)$$

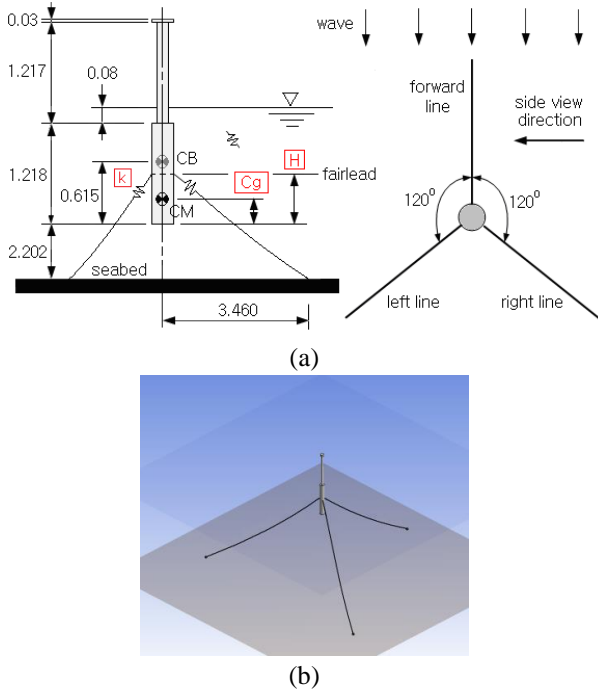


Fig. 3 A simulation problem: (a) simplified moored spar-type platform (scale: 1/75, unit: m) (b) coupled FEM-cable dynamics interaction model

with the boundary conditions given by

$$\dot{\mathbf{u}}_c = 0, \quad \mathcal{G}_c = \mathcal{G}_c^B \quad \text{at } s=0 \text{ (at seabed)} \quad (9)$$

$$\dot{\mathbf{u}}_c = \dot{\mathbf{d}}_p, \quad \mathcal{G}_c = \pi/2 - \mathcal{G}_c^F \quad \text{at } s=L \text{ (at fairlead)} \quad (10)$$

In which, m_c indicates the mass per unit arc length, m_a the added mass of water, $\dot{\mathbf{u}}_c$ and $\dot{\mathbf{d}}_p$ the velocity and platform motion vectors, s the arc length of unstressed cable, and γ the engineering strain. In addition, \mathbf{r}_t is the vector tangent to the cable center line, \mathbf{M}_c and \mathbf{T}_c the resultant internal moment and the resultant tension, and \mathbf{F}_c the external loading per unit arc length due to the self-weight $\rho_c g$. And \mathbf{F}_n , \mathbf{F}_t and \mathbf{F}_q are the normal, tangential and bi-normal drag forces (Morison *et al.* 1950).

3. Numerical simulation and experiment using a scale model

A simplified scale model of 2.5 MW spar-type floating offshore wind turbine with three equal Nylon mooring lines is taken for the numerical and experimental investigation on the platform dynamic response and the mooring tension. All the conditions are kept the same for both the numerical simulation and experiment, and the natural frequencies, the response amplitude operators (RAOs) and the mooring tensions are compared for the sake of reliability assurance.

3.1 A 1/75 scale model of spar-type floating offshore wind turbine

The geometry dimensions, masses and moments of

Table 1 Major specifications of scale platform model

Components	Items	Values
Platform	Total mass	21 kg
	Diameter (upper & lower)	0.076 m, 0.150 m
	Thickness (upper & lower)	2.9 m, 3.2 m
	Pitch moment of inertia	9.240 kg·m ²
	Roll moment of inertia	9.237 kg·m ²
	Yaw moment of inertia	0.065 kg·m ²
Tubular Morison element	Diameter	0.151 m
	Element thickness	1.0×10 ⁻³ m
	Mass density	1.0 kg·m ³

inertia of the major components are given in Fig. 3(a) and Table 1. Three rotor blades, hub and nacelle assembly are modeled as a lumped mass for both numerical simulation and wave tank experiment. For the fluid-rigid body interaction simulation, the whole simplified platform is discretized with the total of 10,465 10-node hexahedron elements. The center of buoyancy (CB), the center of gravity (Cg) and the fairlead location H are measured from the bottom of platform, where the latter two parameters Cg and H are taken variables for the parametric investigation. Three mooring lines are connected to the platform using three equal linear springs with the spring constant k which is also taken variable for the parametric investigation.

In accordance with the dimensions of wave tank, the sectional dimensions of the water pool for the numerical simulation are set by 8×8 m and the water depth is set by 3.5 m, respectively. The total stretched length of three nylon mooring cables and the relative angles between two adjacent mooring lines are set by 4.343 m and 120° respectively. A taut nylon mooring cable is used only for the sake of scale model experiment, because it is normally not recommended for full-scale floating structures. It might experience very large tension loads if the mooring system is designed to restrict the wave frequency vertical motions. Three mooring lines are equally pre-tensioned by 0.49 kgf and the pre-tension is implemented in the numerical simulation by specifying their initial unstretched length L_c^{init} . Each mooring line is discretized into 100 uniform elements and fixed at seabed and connected to the platform by the node-to-node connection. The equivalent cross sectional area A_c , the mass per unit length γ_c , the stiffness EA and the unstretched initial length L_c^{init} are set by 3.14×10⁻⁶ m³, 1.1 kg/m, 2.0×10² N and 4.242 m respectively. The fluid viscous damping effect is reflected by adding a tubular Morison element to the outer surface of the lower wet part of platform, and the associated viscous drag coefficient C_d and added mass coefficient C_{add} are set by 0.75 and 1.0. The Morison force is calculated by $\rho_w D_m C_d (\mathbf{V} - \dot{\mathbf{u}}) |\mathbf{V} - \dot{\mathbf{u}}|$ with ρ_w and D_m being the water density and the characteristic diameter of tubular Morison element (Ansys 2012) which artificially represents the wave damping.

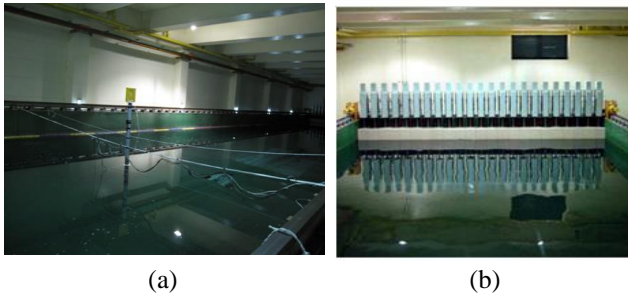


Fig. 4 Experimental setup: (a) scale model in wave tank (b) 1-D wave generator

Table 2 The values taken for the parametric simulation

Items	Fairlead position (m)		Spring constant (N/m)		Center of gravity (m)	
	$H1$	$H2$	$k1$	$k2$	$Cg1$	$Cg2$
Values	0.615	1.135	7.25	11.27	0.448	0.557

3.2 Experimental setup

Figs. 4 and 5 represent the simplified scale model in water tank, 1-D wave generator, and the data acquisition system used for the experiment. The wave tank used for the model test is 100 m in length, 8 m in width, and 3.5 m in depth, and the scale model is moored at 30 m downstream of the wave generator and a wave gauge is used to measure the wave elevation. The ranges of wave height and wave length of the wave generator are 0.05~0.35 m and 0.6~120 m respectively. On the right side of the wave tank, three cameras in the vision system and a data acquisition system are placed. The scale platform model is moored by three mooring lines, and the tension sensors and springs are connected between mooring lines and fairleads. A square plate is installed on the top of platform, where infrared light emit diodes (LEDs) are attached to detect the dynamic motion of platform. The light signals of LEDs are detected by a trinocular vision system, and the six rigid body motions of the floating platform are monitored. In addition, a small-size attitude and heading reference system (AHRS) manufactured by Micro-Electro-Mechanical-Systems Technology is attached on the top of platform to measure the acceleration, angular velocity, and attitude of the scale model. The sensor sends the motion signals to the computer through USB (universal serial bus) port in RS-232 protocol.

The trinocular vision system consists of a trinocular camera, three infrared LEDs (light emit diodes), camera controller, and computer. The vision system, controller, and computer are placed on the side of the wave tank. The vision system monitors three dimensional position and attitude of the square plate. The camera controller sends the signals to the computer through the camera interface card, and the computer calculates the position and attitude of the platform in real time. Tension sensors measure the mooring line tensions, and the sensor signals are generated in the wheatstone bridge type such that the computer acquires the tension signals through a bridge input module. Wave gauge is of capacitive type and immersed in the wave tank to measure the height of water wave. The signal is amplified

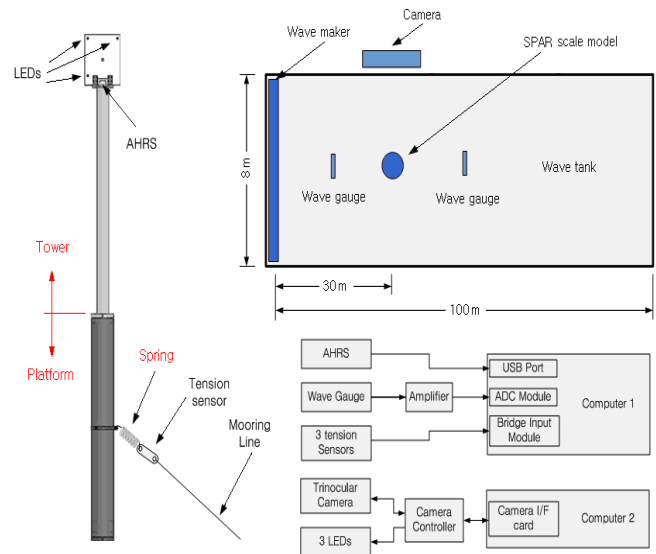


Fig. 5 Composition of data acquisition system

and sent to the computer through an analog to digital converter.

4. Comparison between numerical simulation and experiment

Numerical simulations and water-tank experiments were carried out for the same 1/75 scale model introduced in Section 3. The natural frequencies and the response amplitude operators (RAOs) of the spar-type floating platform and the mooring tensions are analyzed and compared between numerical simulation and experiment. In order for the parametric investigation, the fairlead position H , the spring constant k , and the Cg location of platform are considered as three parameters. And, the detailed values taken for these three parameters are given in Table 2.

4.1 Heave and pitch natural frequencies

Figs. 6(a) and 6(b) comparatively represent the damping ratios in heave and pitch motions, respectively, where $Cg1$ and $Cg2$ stand for two cases of the scale model without the mooring cables. Those were obtained by the panel method that is provided in hydro code. In case of heave motion, the damping ratios of scale model with mooring cables are shown to be higher than the scale model without mooring cables. It is because the draft of moored system is larger than the case of without mooring cables. Meanwhile, it is observed that the damping ratio increases as the Cg location goes up but it slightly decreases as k and H of mooring cables become larger. Meanwhile, in case of pitch motion, it is firstly observed that the damping ratio is independent of the fairlead location H and the damping ratio increases as the Cg location goes up. But, the increase of spring constant k makes the damping ratio smaller, as in case of heave motion.

The heave natural frequencies by numerical simulation and experiment are represented in Fig. 7. First of all, it is

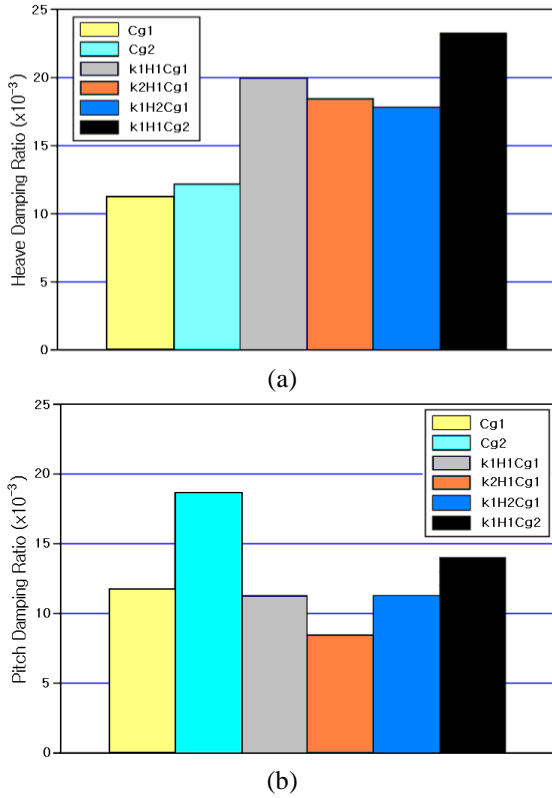


Fig. 6 Comparison of damping ratios: (a) heave, (b) pitch

clearly observed that both methods show an excellent agreement for all the parametric cases. Depending on whether or not the mooring cables are attached, the heave natural frequencies show an apparent difference such that the case without mooring cables leads to much higher natural frequency. The reason can be explained using the approximate heave natural frequency of moored floating body, which is given by

$$\omega_n = \sqrt{(k_b + k_m)/(M + M_a)}, \quad k_b = \rho_w g A_w \quad (11)$$

Here, k_b is the spring constant of buoyancy force, k_m the string constant of mooring system, M the platform mass, M_a the added mass, and A_w the area of waterplane of platform. Referring to Fig. 5, for our scale model, the waterplane passes through the upper tower part when the floating platform is constrained by mooring cables. But it moves downwards to the lower platform part as the floating body moves upwards when mooring cables are not attached. In addition, the added mass M_a slightly decreases as the floating body moves upwards. Hence, the increase of k_b , together with the decrease of M_a , makes the heave natural frequency higher for non-moored floating system, even though k_m is zero. However, this explanation is restricted to only the taut mooring line because the vertical stiffness of taut mooring line is much higher than the hydrostatic stiffness. If a soft catenary mooring line is adopted, it will not affect the heave natural frequency so much when it is attached to the platform, because its vertical stiffness is much smaller than the hydrostatic stiffness. Meanwhile, the variation of heave natural frequency with respect to the three parameters H, k and C_g is shown to be negligible.

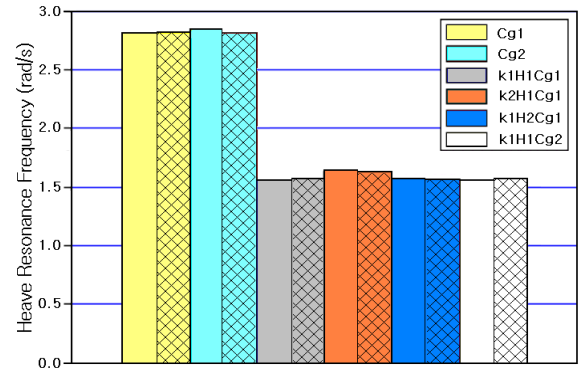


Fig. 7 Comparison of heave natural frequencies (hatched: simulation, non-hatched: experiment)

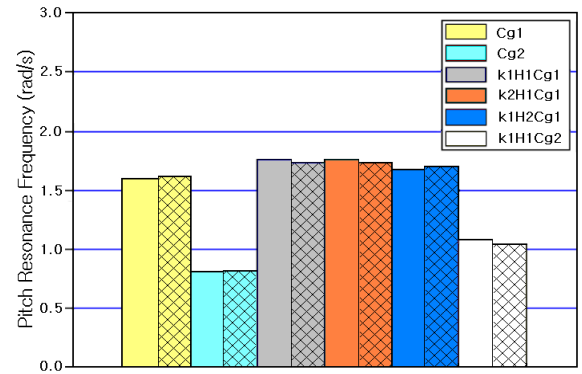


Fig. 8 Comparison of pitch natural frequencies (hatched: simulation, non-hatched: experiment)

The comparison of pitch natural frequencies between the numerical simulation and the experiment is represented in Fig. 8, where an excellent agreement between two methods is also clearly observed. First of all, contrary to the heave motion, the pitch natural frequency becomes slightly higher when the mooring cables are attached to the floating platform. It is because the mooring tension is added to the rotational stiffness of floating platform in the pitch direction. The most apparent fact is that the pitch natural frequency is greatly influenced by the CG location such that it becomes significantly lower as the CG location goes up. It is consistent well with the fact the pitch stiffness decreases as the relative distance between CG and CB (center of buoyancy) becomes shorter (Karimirad *et al.* 2011). Meanwhile, it is observed that the pitch natural frequency becomes slightly lower as the fairlead location H approaches CB such that it approaches the case without mooring cables. In other words, the influence of mooring cable on the pitch natural frequency diminishes as the fairlead location approaches the center of buoyancy.

4.2 RAOs of surge, heave and pitch motions and the mooring tension

Next, the response amplitude operators (RAOs) of the moored floating platform are investigated with respect to three parameters, H, k and C_g . As given in Table 3, four experiments were carried out for each test case, in order to improve the reliability of experiment results. The wave

Table 3 The frequencies and heights of regular wave taken for the experiment

Wave frequencies (rad/s)	Wave heights (cm)			
	k1H1Cg1	k2H1Cg1	k1H2Cg1	k1H1Cg2
2.62	3.46	3.95	2.39	3.20
3.14	3.07	3.51	3.06	3.58
4.19	4.16	4.57		3.45
4.49			4.19	
6.28	4.16	4.51	5.01	4.80

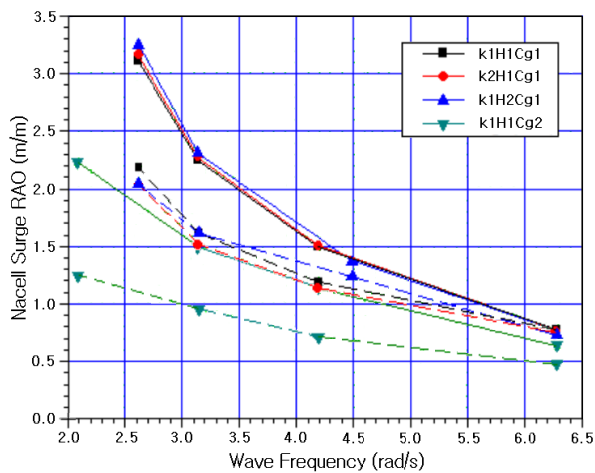


Fig. 9 Comparison of the nacelle surge RAOs (solid line: simulation, dotted line: experiment)

frequencies were selected by considering the natural frequencies of the scale model because the motion of scale model becomes quite irregular and the RAOs of scale model are not easy to determine when the wave frequency is near the natural frequencies of scale model. And, the wave heights were limited to several centimeters. The reliability of the RAOs is evaluated through the comparison between the numerical simulation and the water tank experiment. Referring to Fig. 5, surge, heave and pitch motions were measured at the nacelle position.

Fig. 9 represents the surge RAOs for four parametric cases, where it is observed that the numerical simulation as a whole leads to higher RAOs than the experiment at low frequencies. The reason of this difference is considered to be caused by the wave drifting force in the floating body. The drifting force is large when the wave length is large or wave frequency is low if other conditions are the same. At low wave frequencies, large drifting force causes large movement in the horizontal mean position of the floating body. With this large movement, the coil spring attached to the forward mooring line experiences large mean elongation and its spring constant does also increase. This makes surge RAO relatively small at low frequencies. But, the spring constant change due to the drifting force is not considered in the numerical simulation. Thus, the numerical simulation leads to relatively higher surge RAOs than the experiment at low frequencies.

A prominent feature in both numerical simulation and experiment is that the surge RAO is insensitive to the fairlead position and the cable spring constant k but it is

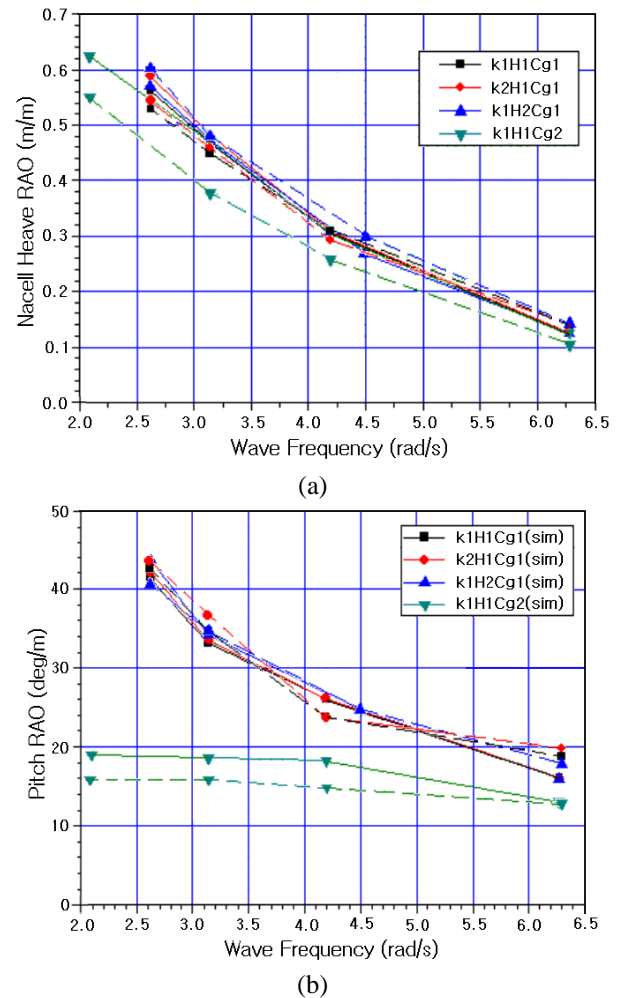


Fig. 10 (a) Nacelle heave RAOs, (b) platform pitch RAOs (solid line: simulation, dotted line: experiment)

greatly affected by the C_g location. From the fact that the surge RAO is measured at the nacelle position, the coupling between surge and pitch motions leads to smaller surge RAO as the C_g location goes up (i.e., approaches to the center of buoyancy).

Figs. 10(a) and 10(b) comparatively represent the heave and pitch RAOs, where the numerical simulations and experiments show a relatively good agreement, differing from the case of surge RAO. In case of the heave RAO, its variation to three parameters H, k and C_g is observed to be insignificant. It is consistent well with the parametric results of heave natural frequency shown in Fig. 7. Thus, it has been justified that both the heave natural frequency and the heave RAO are insensitive to the three parameters. Meanwhile, in case of the pitch RAO, its dependence on the C_g location is clearly observed from Fig. 10(b). In connection with the previous case of surge RAO, the pitch amplitude becomes smaller as the C_g location approaches the center of buoyancy (i.e., the C_g location goes up). Furthermore, it is observed that the variation of pitch RAO to the wave frequency becomes insensitive as the C_g location approaches the center of buoyancy. It implies that the pitch stiffness becomes frequency-independent when the relative distance between C_g and CB becomes smaller than

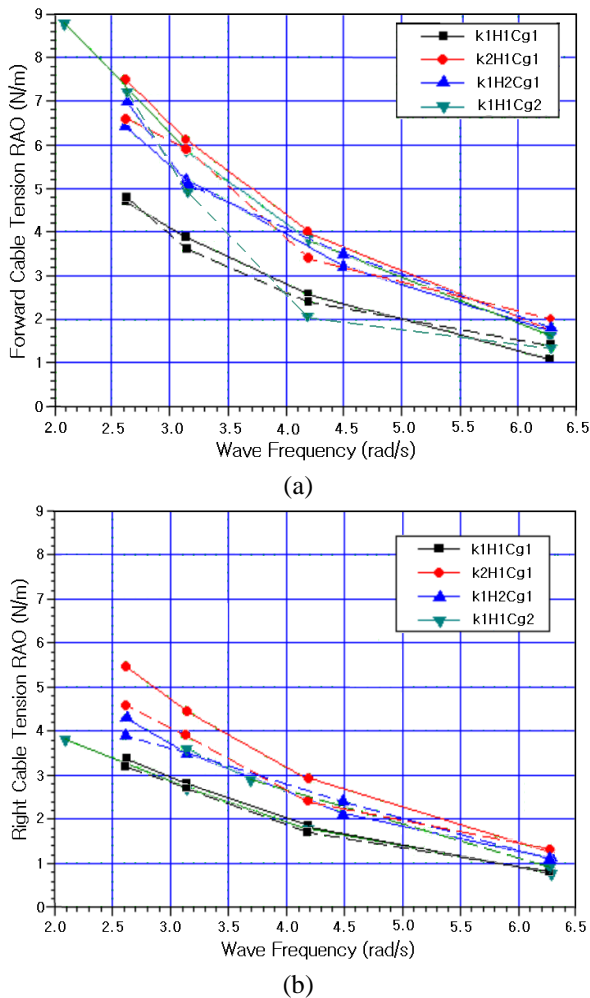


Fig. 11 Comparison of the mooring tension RAOs: (a) front cable, (b) right cable

a certain critical value. In case of the fairlead position, it has been reported that it affects the pitch motion (Jeon *et al.* 2013) such that the pitch motion becomes smaller as the position goes up above the center of buoyancy. The experiment shows the similar trend as a whole, but the simulation does not. Meanwhile, the effect of spring constant is observed to be negligible, implying that its value is low to affect the platform motion (Loukogeorgaki and Angelides 2005).

We next investigated the dependence of mooring tension in RAO on the three parameters H , k and C_g . Since the right and left mooring cables are symmetric each other with respect to the wave direction as shown in Fig. 3(a), the mooring tension of the left cable is excluded. Fig. 10 compares the mooring tension RAOs of the front and right cables between the numerical simulation and experiment. First of all, it is observed, from the comparison between Figs. 11(a) and 11(b), that the front cable produces higher tension than the right cable, which is consistent well with the fact that the front cable aligned in the wave direction experiences larger extension. The fact that the mooring cables aligned in the wave direction produce higher mooring tension was also reported in the previous work by Jeon *et al.* (2013). Meanwhile, it is clearly observed that the

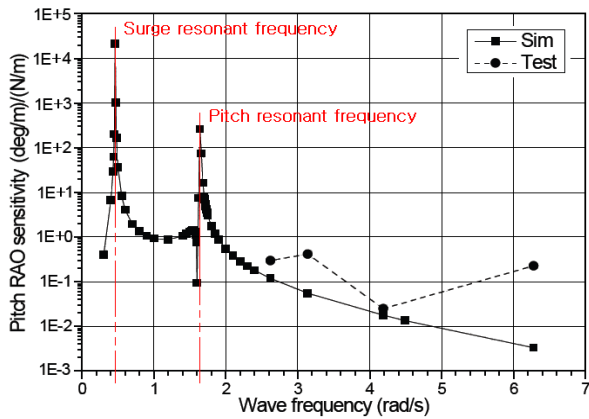
numerical simulation and experiment shows a consistent trend to some extent, which implies that the inherent dynamic effect of mooring cables is appropriately reflected in the numerical simulation.

In both cables, the mooring tension increases in proportional to the spring constant k , which does make sense from the physical point of view. In addition, it does also increase as the fairlead position H goes up, which is consistent with our previous study on the mooring tension (Jeon *et al.* 2013). The suspended portion of mooring cable becomes larger as the fairlead position goes up if both the total cable length and the anchor position at seabed are kept the same, and such an increase of the cable suspended portion makes the cable tension higher. Regarding the C_g position, the mooring tension shows the similar trend to the other two parameters only for the front cable by the numerical simulation and the right cable by experiment. But, the numerical simulation for the right cable does not show any increase and the mooring tension by experiment for the front cable shows an increase only at lower frequency, to the increase of C_g position (i.e., from C_{g1} to C_{g2}). As a whole, the mooring tension is observed to be lowest in case of $k1H1Cg1$.

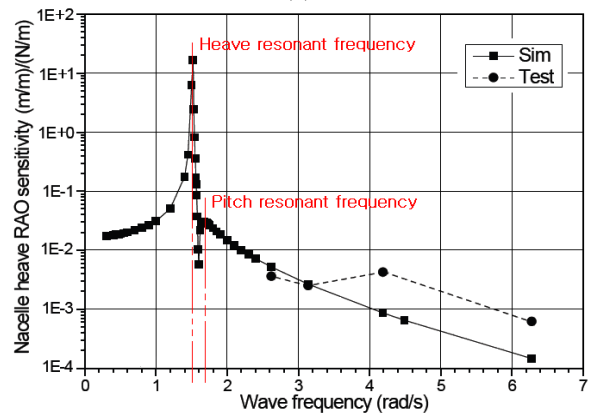
4.3 Sensitivity to the mooring system

Next, the sensitivities of surge, pitch and heave motions to the change of mooring system were investigated numerically and experimentally. In case of numerical simulation, the sensitivities were calculated by the hydro code with small perturbations of the spring constant k and the fairlead position H for the test condition $k1H1Cg1$. Meanwhile, for the experiment, the sensitivities were determined from RAOs of four test conditions given in Table 3. For example, the pitch sensitivity to the spring constant k was determined from the ratio of the difference between pitch RAOs for $k2H1Cg1$ and $k1H1Cg1$ with respect to the difference of spring constant ($k_2 - k_1$). The sensitivities of scale model RAO to the spring constant and the fairlead positions are represented in Figs. 12 and 13, respectively. The sensitivity of surge RAO is excluded because it was almost similar to one of pitch RAO.

From the comparison between Figs. 12(a) and 13(a), it is found that the pitch RAO is more sensitive to the fairlead position. But, the sensitivities of heave RAO in Figs. 12(b) and 13(b) to two mooring parameters are shown to be almost similar. Meanwhile, In case of pitch RAO, two peaks are observed at the surge and pitch resonant frequencies, while in case of heave RAO, one peak is apparent at its resonant frequency but another peak at the pitch resonant frequency is negligible. This distinct difference is caused by the coupling characteristics of three platform motions. For a small wave height and negligible viscous effect, the dynamic equations for surge, pitch and heave motions of the scale model with 180° heading can be expressed by two separated linear second-order differential equations, one for the coupled surge and pitch motion and the other for the heave motion (Newman 1977). In other words, surge and pitch exhibit a strong coupling in their resonant responses, but the coupling between heave and surge/pitch is negligible.

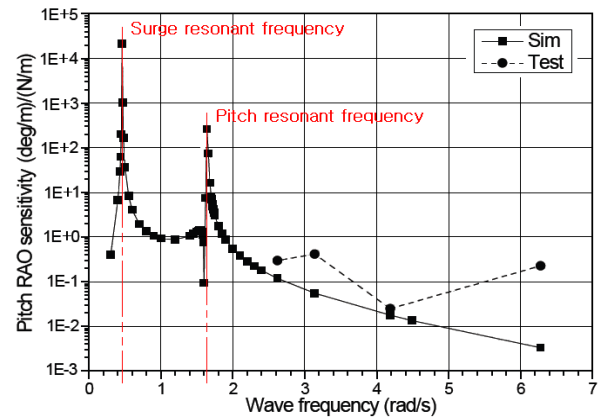


(a)

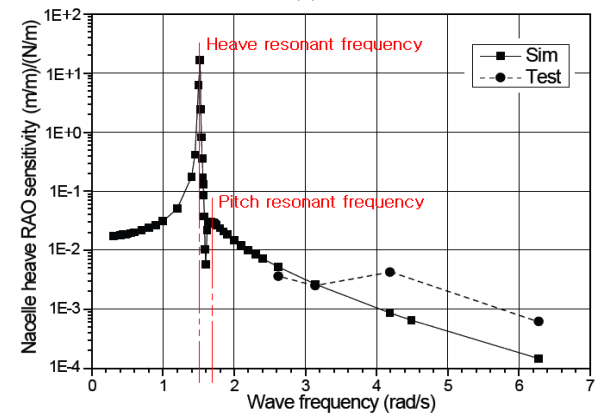


(b)

Fig. 12 Sensitivity to the spring constant k : (a) pitch RAO, (b) nacelle heave RAO



(a)



(b)

Fig. 13 Sensitivity to the fairlead position H : (a) pitch RAO, (b) nacelle heave RAO

On the other hand, it is observed from the figures that the experimental test and numerical simulation result are similar each other to some extent. The discrepancy between the experiment and simulation, particularly in the higher frequency range, is considered to be caused by the error in RAO measurement.

5. Conclusions

This paper addressed the comparative numerical and experimental study on the natural frequencies and the dynamic responses in RAO to 1-D regular wave of a simplified moored 1/75 scale model of spar-type floating offshore wind turbine. A fluid-cable dynamics interaction method was employed for the numerical simulation, while a wave tank equipped with the specially-designed vision and data acquisition system was set up for the experiment. The fairlead position, the spring constant and the location of center of mass were selected as three key design parameters, and four test cases were chosen by appropriately combining these key parameters. Through the numerical simulation and experiment, the results of four test cases were compared and investigated. As well, the sensitivities of RAOs to the mooring system were investigated. Through the comparative and parametric simulations and experiments, the following main observations are drawn

- First of all, the numerical simulation and experiment shows a good agreement, except for the nacelle surge RAOs. In case of surge motion, the numerical simulation leads to higher RAOs than the experiment at low frequencies, because the tubular Morison element used for the numerical simulation cannot appropriately reflect the restoring force of mooring lines at low frequencies.
- In case of heave natural frequency, its dependence on the three parameters H , k and C_g is negligible. But, the pitch natural frequency is greatly influenced by the C_g location such that it becomes significantly lower as the C_g location goes up. Meanwhile, the pitch natural frequency becomes slightly lower as the fairlead location H approaches the center of buoyancy. The surge RAO is insensitive to the fairlead position and the cable spring constant k but it becomes lower as the C_g location goes up.
- In case of mooring tension, the front cable produces higher mooring tension than the right cable because it is aligned in the direction of wave. Meanwhile, to the three parameters, the mooring tension increases in proportional to the spring constant k and as the fairlead position H and the C_g position go up as a whole.
- The heave RAO shows almost the same sensitivity to the fairlead position and the spring constant, but the pitch and surge RAOs are more sensitive to the fairlead

position. Meanwhile, pitch and surge show the coupled resonance responses to each other, but heave does show the coupling with pitch and surge.

References

- Aamo, O.M. and Fossen, T.I. (2000), "Finite element modeling of mooring lines", *Math. Comput. Simul.*, **53**(4-6), 415-422.
- ANSYS AQWA (2012), Available from: <http://www.ansys.com/products/aqwa/>.
- Cho, J.R., Lee, H.W. and Ha, S.Y. (2005), "Finite element analysis of resonant sloshing response in 2-D baffled tank", *J. Sound Vib.*, **288**, 829-845.
- Choi, E.Y., Cho, J.R., Cho, Y.U., Jeong, W.B., Lee, S.B., Hong, S.P. and Chun, H.H. (2015), "Numerical and experimental study on dynamic response of moored spar-type scale platform for floating offshore wind turbine", *Struct. Eng. Mech.*, **54**(5), 909-922.
- Colwell, S. and Basu, B. (2009), "Tuned liquid column dampers in offshore wind turbines for structural control", *Eng. Struct.*, **31**, 358-368.
- Dinh, V.N., Basu, B. and Nagarajaiah, S. (2016), "Semi-active control of vibrations of spar-type floating offshore wind turbines", *Smart Struct. Syst.*, **18**(4), 683-7005.
- Dodaran, A.A. and Park, S.K. (2012), "Development of design static property analysis of mooring system caisson for offshore floating wind turbine", *Int. J. Ocean Syst. Eng.*, **2**(2), 97-105.
- Faltinsen, O.M. (1990), *Sea Load on Ships and Offshore Structures*, University of Cambridge.
- Fowler, M.J., Kimball, R.W., Thomas Iii, D.A. and Goupee, A.J. (2013), "Design and testing of scale model wind turbines for use in wind/wave basin model tests of floating offshore wind turbines", *Proceedings of the ASME 2013 32nd International Conference Ocean, Offshore and Arctic Engineering*, OMAE2013-10122, Nantes, France, June.
- Goodman, T.R. and Breslin, J.P. (1976), "Statics and dynamics of anchoring cables in waves", *J. Hydronaut.*, **10**(4), 113-120.
- Goupee, A.J., Koo, B.J., Lambrakos, K.F. and Kimball, R.W. (2012), "Model tests for three floating wind turbine concepts", *Proceedings of the Offshore Technology Conference*, Houston, USA.
- Jensen, J., Olsen, A. and Mansour, A. (2011), "Extreme wave and wind response predictions", *Ocean Eng.*, **38**, 2244-2253.
- Jeon, S.H., Cho, Y.U., Seo, M.W., Cho, J.R. and Jeong, W.B. (2013), "Dynamic response of floating substructure of spar-type offshore wind turbine with catenary mooring cables", *Ocean Eng.*, **72**, 356-364.
- Jonkman, J. (2009), "Dynamics of offshore floating wind turbines-model development and verification", *Wind Energy*, **12**, 459-492.
- Jonkman, J. and Musial, W. (2010), "Offshore code comparison collaboration (OC3) for IEA task 23 offshore wind technology and development", Technical Report NREL/TP-5000-48191, Colorado.
- Karimirad, M. (2010), "Dynamic response of floating wind turbines", *Trans. B: Mech. Eng.*, **17**(2), 146-156.
- Karimirad, M., Meissonnier, Q., Gao, Z. and Moan, T. (2011), "Hydroelastic code-to-code comparison for a tension leg spar-type floating wind turbine", *Marine Struct.*, **24**, 412-435.
- Koo, B.J., Kim, M.H. and Randall, R.E. (2004), "Mathieu instability of a spar platform with mooring and risers", *Ocean Eng.*, **31**, 2175-2208.
- Lee, H.H., Wong, S.H. and Lee, R.S. (2006), "Response mitigation on the offshore floating platform system with tuned liquid column damper", *Ocean Eng.*, **33**, 1118-1142.
- Lee, K.H. (2005), "Response of floating wind turbines to wind and wave excitation", Masters Thesis, MIT.
- Lee, S.H. (2008), "Dynamic response analysis of spar buoy floating wind turbine systems", Ph.D. Thesis, MIT.
- Loukogeorgaki, W. and Angelides, D. (2005), "Stiffness of mooring lines and performance of floating breakwater in three dimensions", *Appl. Ocean Res.*, **27**(4-5), 187-208.
- Martin, H.R., Kimball, R.W., Viselli, A.M. and Goupee, A.J. (2012), "Methodology for wind/wave basin testing of floating offshore wind turbines", *Proceedings of the ASME 2012 31st International Conference Ocean, Offshore and Arctic Engineering*, OMAE2012-83627, Rio de Janeiro, Brazil, July.
- Morison, J.R., O'Brien, M.P., Johnson, J.W. and Schaaf, S.A. (1950), "The force exerted by surface waves on piles", *Petroleum Tran.*, **189**, 149-157.
- Mostafa, M., Murai, M., Nishimura, R., Fujita, O. and Nihei, Y. (2012), "Experimental validation for motion of spar-type floating wind turbine at inclination with effect of gyro moment of the rotating blade of windmill", *Proceedings of the International Offshore Polar Engineering Conference*, Rhodes, Greece.
- Newman, J.N. (1977), *Marine Hydrodynamics*, MIT Press, Cambridge.
- Patel, M.H. (1989), *Dynamics of Offshore Structures*, Butterworths, London.
- Sannasiraj, S.A., Sundar, V. and Sundaravadelu, R. (1998), "Mooring forces and motion responses of pontoon-type floating breakwaters", *Ocean Eng.*, **25**(1), 27-48.
- Shin, H. and Dam, P. (2012), "Model test of a floating offshore wind turbine moored by a spring-tensioned leg", *Proceedings of the International Offshore Polar Engineering Conference*, Rhodes, Greece.

CC